Z. Kristallogr. **2012**, *227*, 280–287 / **DOI** 10.1524/zkri.2012.1503
© by Oldenbourg Wissenschaftsverlag, München

Reverse Monte Carlo study of apical Cu–O bond distortions in $YBa_2Cu_3O_{6.93}$

Callum A. Young[I], Edward Dixon[I], Matthew G. Tucker[II], David A. Keen[II], Michael A. Hayward[I] and Andrew L. Goodwin*,[I]

[I] Department of Chemistry, University of Oxford, Inorganic Chemistry Laboratory, South Parks Road, Oxford, OX1 3QR, U.K.
[II] ISIS Facility, Rutherford Appleton Laboratory, Harwell Oxford, Didcot, OX11 0QX, U.K.

Received December 12, 2011; accepted January 27, 2012

Pair distribution function / Reverse Monte Carlo / High-temperature superconductivity / Yttrium barium copper oxide / Local structure

Abstract. A combination of neutron total scattering measurement and reverse Monte Carlo (RMC) refinement is applied to the study of apical Cu–O bond distortions in the high-T_c superconductor $YBa_2Cu_3O_{6.93}$. We show that the average structure is not consistent with a split-site model for the corresponding Cu and O positions, but that the local structure nevertheless reveals the existence of two separate apical Cu–O bond lengths. Using $G(r)$ data obtained from a variety of Q_{max} values we show that this result is independent of the data treatment methodology. We also find that the resulting 'short' and 'long' Cu–O bond lengths agree well with the results of previous EXAFS studies. The existence of bimodal apical Cu–O bond distributions in the context of a single-site average structure model is interpreted in terms of correlated displacements of the Cu and O atoms. We investigate the possibility of clustering of short apical Cu–O bonds within our RMC configurations.

1. Introduction

The mechanistic role of structural inhomogeneities has remained a contentious aspect [1–3] of the science of high-temperature superconductors almost since the phenomenon was first discovered – be it in the form of electron-phonon coupling [4], charge localisation ('stripes') [5] or bipolaron formation and condensation [6]. Local-structure probes, such as X-ray absorption spectroscopy and total scattering (or pair distribution function, PDF) measurements, might be expected to be particularly sensitive to the extent and nature of lattice distortions, and yet the results of such experiments have often appeared contradictory and remain controversial. As a consequence there exists no generally-accepted microscopic description of local structure distortions in canonical high-T_c materials such as the $YBa_2Cu_3O_{7-\delta}$ (YBCO) family.

In the particular case of YBCO, it is the existence of a double-well potential for the apical Cu2–O4 bond that has proven particularly contentious, primarily because of the associated implications for charge localisation and electron-lattice coupling (Fig. 1a) [7]. An early XANES study was the first to suggest the existence of such a double-well [8], and a number of EXAFS investigations in the intervening years have essentially supported this same conclusion [9–13]. In contrast, both single crystal [14, 15] and powder [16–19] diffraction experiments found no evidence for splitting of either the Cu2 or O4 crystallographic sites. Likewise neutron PDF studies ruled out a bimodal distribution of O4 positions but yielded improved fits for models that allowed a variety of different splittings of the Cu2 site [20, 21]. And whereas frozen-phonon *ab initio* calculations failed to reproduce a double-well potential for the Cu2–O4 bond [22], inelastic neutron scattering measurements linked an increased sensitivity of the dynamic scattering function $S(Q,E)$ near T_c to structural instabilities involving shortening of the same bond [23].

In this paper we attempt to rationalise some of these apparently contradictory results by carrying out a reverse Monte Carlo (RMC) refinement of newly-collected neutron total scattering data for a carefully synthesised YBCO sample of composition $YBa_2Cu_3O_{6.93}$. This is very much a PDF study, but there are two key differences between our approach and those of Refs. [20, 21]. First, where these previous studies have focussed on interpreting structural features of the PDF in terms of increasingly complex single-particle correlations – through symmetry lowering of the unit cell or the introduction of split sites – RMC refinement allows the PDF to be interpreted in terms of *correlated* displacements of atoms. Second, our RMC refinements include simultaneous fits to both PDF and Bragg intensity data, a process that ensures the resultant atomistic configurations are automatically consistent with traditional average-structure refinements. The key result of our study is that the Cu2–O4 bond distribution in our RMC configurations is indeed bimodal, but that correlations between the Cu2 and O4 displacements result in uni-

* Correspondence author
(e-mail: andrew.goodwin@chem.ox.ac.uk)
For Supplementary Material see online-version.

This article is protected by German copyright law. You may copy and distribute this article for your personal use only. Other use is only allowed with written permission by the copyright holder.

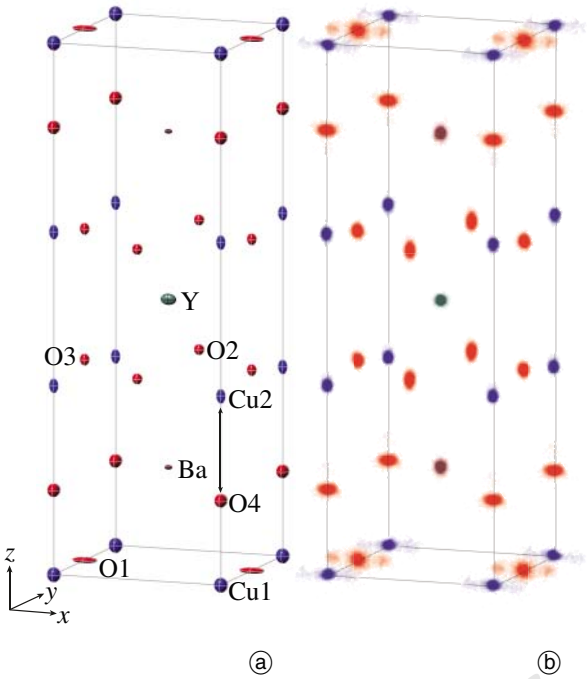

Fig. 1. Representations of the average structure of $YBa_2Cu_3O_{6.93}$ determined by (**a**) Rietveld refinement and (**b**) RMC refinement of neutron total scattering data. The crucial Cu2−O4 bond is indicated by the arrow. Thermal ellipsoids in (**a**) are shown at 80% probability level; the representation in (**b**) is obtained by projecting the RMC configuration onto a single unit cell.

modal distributions for both Cu2 and O4 sites. In this way, we are able to rationalise the apparent discrepancy amongst EXAFS, PDF and average structure crystallographic studies.

2. Materials and methods

2.1 Synthesis and characterisation

A sample of $YBa_2Cu_3O_{7-\delta}$ (2.5 g) was prepared via the citrate gel route described previously [24]. A suitable stoichiometric mixture of Y_2O_3 (99.999%, dried at 900 °C), $BaCO_3$ (99.997%) and CuO (99.9999%) was dissolved in a minimum quantity of 6 M nitric acid. Four mole equivalents of citric acid and 4 ml of ethylene glycol were then added and the solution heated with constant stirring. The gel formed was subsequently ground into a fine powder, placed in a crucible lined with Ni foil, and heated in air to 600 °C at a rate of 1 °C min^{-1}. The resulting powder was re-ground and pressed into 13 mm pellets under a force of 5 t. All subsequent heating was performed with the sample contained within an alumina boat lined with Ni foil. The sample was fired at 920 °C under flowing O_2 and then cooled to room temperature at a rate of 1 °C min^{-1}. This process was iterated three times. After the final cooling cycle, the pellets were re-ground and the resulting powder heated at 600 °C for 12 h under flowing O_2 to give a sample with O substoichiometry $\delta = 0.07(3)$ as determined by iodometric analysis. Phase purity was confirmed by X-ray powder diffraction; the refined lattice parameters were found to be in good agreement with previously published values [25]. A measurement of the superconducting transition temperature by SQUID magnetometry gave $T_c = 92(1)$ K.

2.2 Neutron total scattering

Neutron total scattering data were collected using the GEM instrument at ISIS [26–28]. A sample of polycrystalline $YBa_2Cu_3O_{6.93}$ (1.8 g), prepared as described above, was placed within a cylindrical thin-walled vanadium can of 3 mm diameter and 5.8 cm height, which was in turn loaded inside a closed cycle helium refrigerator. The sample was cooled to 50 K and total scattering data then collected over a large range of scattering vectors of magnitudes $0.7 \leq Q \leq 50$ Å^{-1}, corresponding to a real-space resolution of order $\Delta r \simeq 3.791/Q_{max} \simeq 0.08$ Å.

Following their collection, the total scattering data were corrected using standard methods, taking into account the effects of background scattering, absorption, multiple scattering within the sample, beam intensity variations, and the Placzek inelasticity correction [29]. These corrected data were then converted to experimental $F(Q)$ and $G(r)$ functions [29, 30]:

$$F(Q) = \varrho_0 \int_0^\infty 4\pi r^2 G(r) \frac{\sin Qr}{Qr} \, dr \,, \tag{1}$$

$$G(r) = \sum_{i,j} c_i c_j \bar{b}_i \bar{b}_j [g_{ij}(r) - 1] \,, \tag{2}$$

where

$$g_{ij}(r) = \frac{n_{ij}(r)}{4\pi r^2 \, dr \, \varrho_0 c_j} \,, \tag{3}$$

$n_{ij}(r)$ the number of pairs of atoms of type i and j separated by distance r, ϱ_0 is the number density, c_i the concentration of each species i and b_i the corresponding neutron scattering length. As part of the data normalisation process it is usual practice to determine a useable value Q_{max} that represents the best possible compromise between optimising Δr for PDF refinement (*i.e.* making Q_{max} as large as possible) and avoiding the unnecessary inclusion of high-frequency noise that can plague high-Q data. In this instance, we found that a value $Q_{max} = 40$ Å^{-1} produced the most reliable $G(r)$ function.

The Bragg profile functions for each data set were extracted from the scattering data collected by the detector banks centred on scattering angles $2\theta = 54.46°$, $63.62°$ and $91.37°$. The experimental Bragg diffraction profiles were fitted with the GSAS Rietveld refinement program [31] using the published structural model [32]; the fitting process is discussed in greater detail in the Results section below.

2.3 Reverse Monte Carlo refinement

The reverse Monte Carlo refinement method as applied to crystalline materials, together with its implementation in the program RMCProfile have been described in detail elsewhere [29, 33]. The basic refinement objective is to produce large atomistic configurations that can account simultaneously for the experimental $F(Q)$, $G(r)$ and Bragg

This article is protected by German copyright law. You may copy and distribute this article for your personal use only. Other use is only allowed with written permission by the copyright holder.

Table 1. 'Distance window' parameters d_{min}, d_{max} used for all RMC refinements in this study. $\bar{d}$ and $\sigma(d)$ give the final refined peak positions and standard deviations.

Atom pair	d_{min} (Å)	d_{max} (Å)	$\bar{d}$ (Å)	$\sigma(d)$ (Å)
Y−O2,3	2.10	2.56	2.38	0.07
Ba−O	2.50	3.50	2.76	0.13
Cu1−O1	1.73	2.10	1.93	0.06
Cu1−O4	1.73	2.50	1.84	0.04
Cu2−O2	1.73	2.10	1.93	0.06
Cu2−O3	1.73	2.10	1.93	0.06
Cu2−O4	1.73	2.50	2.29	0.06

profile $I(t)$ functions. This is achieved by accepting or rejecting random atomic moves subject to the metropolis Monte Carlo algorithm, where in this case the Monte Carlo acceptance criterion is determined by the quality of the fits to data. The refinement process is continued until no further improvements in the fits to the data are observed. By virtue of the particular importance in the present study of fitting accurately the lowest-r region of the PDF – which includes the all-important distribution of Cu2−O4 separations – we applied a larger weighting to the region $0 \leq r \leq 7$ Å than to the remainder of the PDF.

Our starting configurations for the RMC process were based on a $24 \times 24 \times 8$ supercell of the crystallographic unit cell shown in Fig. 1a. Each configuration contained 59 904 atoms and extended approximately 90 Å in each direction. By virtue of the small experimental value of δ for our sample, and in order to avoid introducing model bias, we did not incorporate any explicit consideration of O vacancies. In addition to the required fits to data, the only constraints placed on the atomic coordinates were a set of 'distance window' constraints which act to maintain an appropriate framework connectivity throughout the refinement process [33, 34]. In each case the values used (see Table 1) were based on the extrema of the corresponding peaks in the experimental PDF.

3. Results

3.1 Average structure determination

Our first step was to use the GSAS refinement package [31] to verify that the Bragg contribution to our total scattering data could be interpreted in terms of sensible lattice parameters, atomic coordinates and anisotropic displacement parameters. The values obtained, which are summarised in Table 2, are in good agreement with previous crystallographic studies of nearly-stoichiometric YBCO samples [15, 18, 32]. The corresponding fits to data are shown in Figs. 2a and S1 (see SI), and a representation of the structural model obtained is that shown in Fig. 1a. It was possible to achieve stable refinement of anisotropic displacement parameters for all atoms other than Ba, for which unconstrained refinement consistently yielded non-positive definite values for the U_{22} parameter; consequently this value was fixed at 0.001 Å^2. We remark also

Table 2. Crystallographic parameters, atomic coordinates and isotropic equivalent displacement parameters determined using Rietveld refinement of neutron scattering data for $YBa_2Cu_3O_{6.93}$.

Crystal system	Orthorhombic			
Space group	*Pmmm*			
a (Å)	3.81412(5)			
b (Å)	3.87694(6)			
c (Å)	11.63970(22)			
V (Å^3)	172.117(3)			
Z	1			
T (K)	50			
Atom	x	y	z	U_{iso} (Å^2)
Y	0.5	0.5	0.5	0.0031(4)
Ba	0.5	0.5	0.18377(12)	0.00092(26)
Cu1	0	0	0	0.0038(4)
Cu2	0	0	0.35535(9)	0.0019(8)
O1	0	0.5	0	0.0115(7)
O2	0.5	0	0.37837(13)	0.0045(4)
O3	0	0.5	0.37727(15)	0.0020(4)
O4	0	0	0.15879(11)	0.0047(4)

This article is protected by German copyright law. You may copy and distribute this article for your personal use only. Other use is only allowed with written permission by the copyright holder.

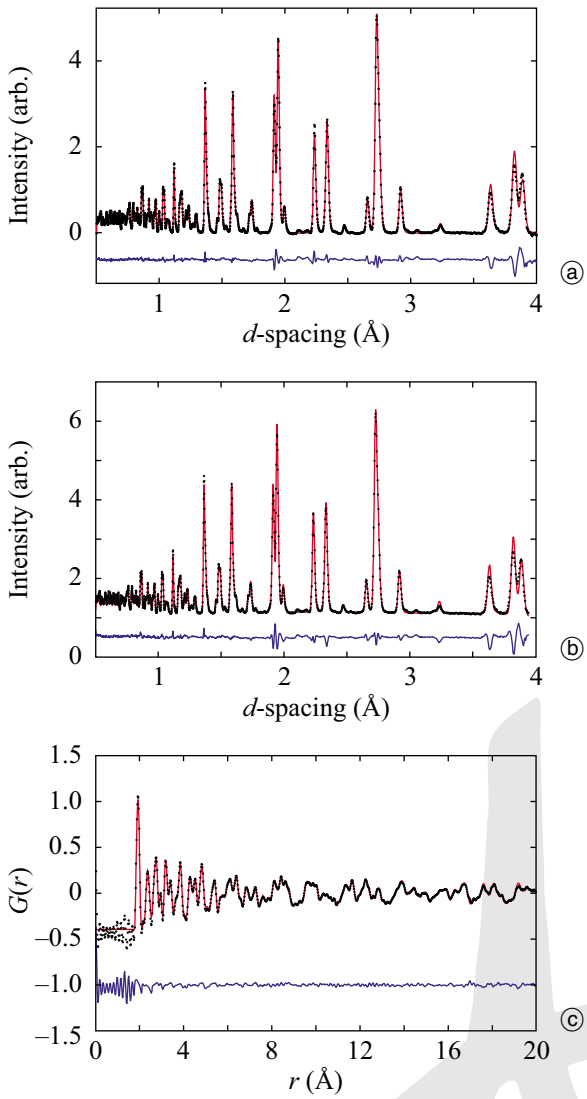

Fig. 2. The fit to neutron powder diffraction data obtained by (**a**) Rietveld and (**b**) RMC refinement. (**c**) The corresponding $G(r)$ fit obtained using RMC. In all cases, data are shown as filled circles, fits as red lines and the difference (data−fit) as blue lines, shifted vertically for clarity. A refined background function has been subtracted from the data and fit shown in (a).

that displacements of the so-called 'chain' oxygen atoms (O1) are clearly very anisotropic. This behaviour, which has been reported elsewhere [15, 21, 25], is thought to be related to low-energy correlated displacements of the Cu1-centred $[CuO_4]$ square units.

Since our study concerns primarily the distribution of Cu2−O4 bonds, we investigated the validity of structural models which incorporated splitting of one or other or both of the two atomic sites. As in previous Rietveld studies [16–19], we found that none of these three models yielded a stable refinement.

3.2 Local structure determination

RMC refinement gave equally satisfactory fits to the neutron scattering data, both in terms of the reciprocal-space Bragg intensity function $I(t)$ and the real-space $G(r)$ transform. Importantly, the quality of the Bragg profile fit is comparable to that obtained from Rietveld refinement, implying that the RMC configurations are as consistent with the Bragg component to the total scattering function as the average-structure model given in Table 2.

By collapsing the atomic coordinates of an entire RMC configuration onto a single unit cell, it is possible to visualise the RMC-refined average structure (Fig. 1b). As found in the Rietveld model, the O1 distribution is anisotropic (and indeed there is some sign here of a split site, although we do not pursue this possibility further here). Encouragingly, the Ba site is now represented by a physically sensible distribution function.

Because the RMC-refined distributions of atomic positions are not constrained to assume ellipsoidal forms, we are able to check in a straightforward and unbiased manner whether or not there is any real evidence for splitting on either the Cu2 or O4 sites. In both instances a projection of the corresponding atomic coordinates onto the z axis gave distributions that could be well fitted using single Gaussian functions. Hence we can say that our RMC refinements are consistent with unimodal single-particle correlation functions for both atom sites. In particular, there can be no need to invoke split Cu2/O4 atom sites in order to fit the neutron scattering data since RMC would have been free to do so should the data have demanded.

With the RMC description of average structure in $YBa_2Cu_3O_{6.93}$ established, we turned our attention to the pair correlations at the heart of the local structure controversy. It is straightforward to calculate from an RMC configuration the distribution functions for specific bonding interactions. Carrying out such a calculation for the crucial apical Cu2−O4 bonds yields a distribution that is quite obviously bimodal (Fig. 3a left-hand panel). The distribution is well fitted using a sum of two Gaussian components, ascribable to contributions from 'short' and 'long' Cu2−O4 bonds. The midpoints of these Gaussian fits suggested a pair of Cu2−O4 bond lengths that were surprisingly similar to the values obtained in the EXAFS study of Ref. [12]: $r_{Cu2-O4} = 2.167$ and 2.307 Å (RMC) *vs* $r_{Cu2-O4} = 2.220$ and 2.337 Å (EXAFS).

We were interested to establish the origin of this feature in the experimental $G(r)$ function in order to determine the extent to which the close agreement with EXAFS results is fortuitous. There is a clear peak in the $G(r)$ function responsible for splitting the Cu2−O4 distribution (Fig. 4a). The only non-zero partial pair distribution function in this particular region is $g_{Cu2,O4}(r)$. All other Cu−O bonds are much shorter and contribute to the first significant peak seen at $r \simeq 1.9$ Å. There is some overlap at higher values of r between the Cu2−O4 and Y−O2/Y−O3 partial pair distribution functions, but the values of $g_{Y,O2}(r)$ and $g_{Y,O3}(r)$ are essentially zero for $r < 2.20$ Å, despite the RMC constraints allowing Y−O distances to be as small as 2.10 Å. Consequently the $r \simeq 2.15$ Å feature in the $G(r)$ function − if real − can be ascribed only to a separate distribution of short Cu2−O4 bonds, and hence is an experimental indication of the existence of a bimodal Cu2−O4 bond distribution.

However, the key question here is whether or not the feature is indeed real − our concern being that its magnitude is comparable to the size of the Fourier truncation ripples evident at the lowest values of r. Although Fourier

This article is protected by German copyright law. You may copy and distribute this article for your personal use only. Other use is only allowed with written permission by the copyright holder.

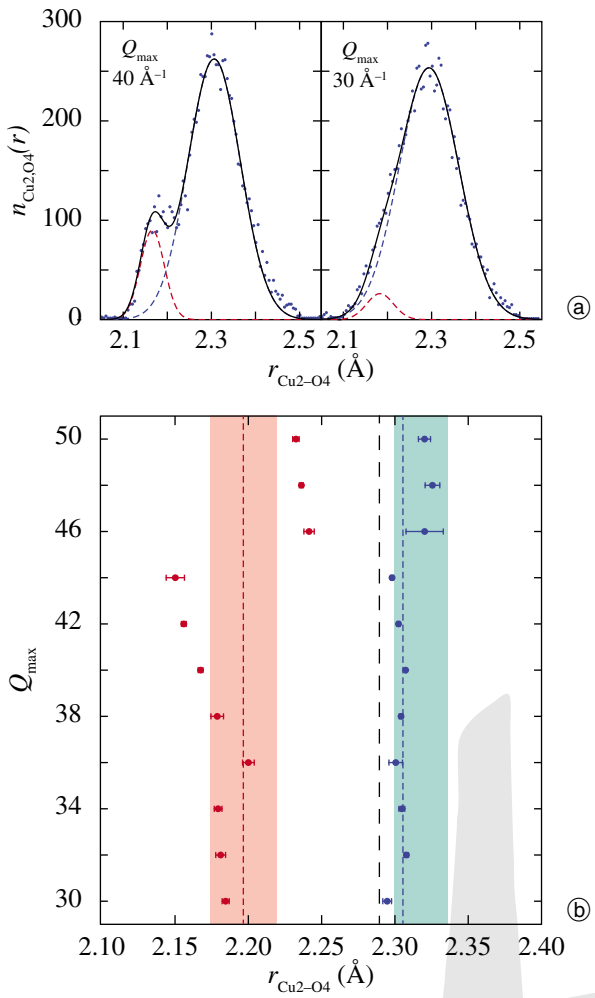

Fig. 3. (**a**) Cu2−O4 bond histograms (solid points) determined by RMC refinements against $G(r)$ functions generated for maximum scattering vectors of (left) $Q_{max} = 40$ Å^{-1} and (right) $Q_{max} = 30$ Å^{-1}. These two distributions correspond respectively to the most and the least convincing bimodal distributions obtained for the 11 different Q_{max} values investigated. Calculated fits using a pair of Gaussian curves are shown as a solid line, with the two individual Gaussian contributions shown as red and blue dashed lines. (**b**) Q_{max}-dependence of the 'short' and 'long' Cu2−O4 bond lengths (red and blue circles, respectively), determined as the midpoints of the corresponding Gaussian fits. Error-weighted averages are plotted as vertical red and blue dashed lines. The range of values obtained using EXAFS in Refs. [10, 12] are shown as shaded regions, with the Rietveld Cu2−O4 bond length value shown as a bold black dashed vertical line.

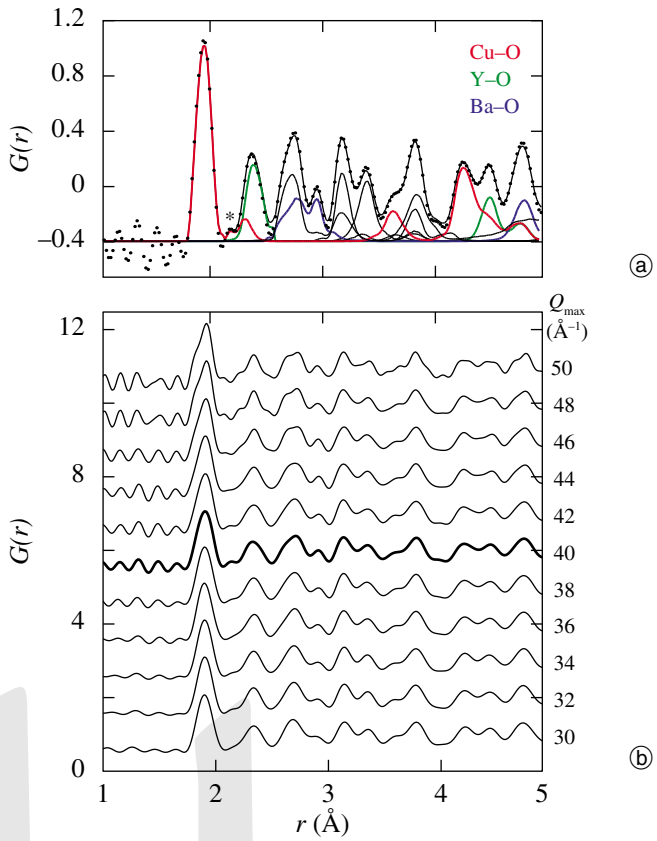

Fig. 4. (**a**) Experimental $G(r)$ function (filled circles) and corresponding RMC fit (solid black line). The relative contributions to the RMC fit arising from the various partial pair distribution functions are included, with those corresponding to the Cu−O, Y−O and Ba−O pairs highlighted in red, green and blue, respectively. The experimental feature responsible for splitting the Cu2−O4 distribution is highlighted with an asterisk. (**b**) Experimental $G(r)$ functions generated using a range of Q_{max} values $30 \leq Q_{max} \leq 50$ Å^{-1}; the bold curve is that shown in (a).

ripples are always strongest at low-r [35], they are present throughout the PDF and it is inevitable that the refinement will fit to some intensity that has no physical origin. The Fourier ripples are generally small compared to the principal peaks in the PDF, and the presence of other data sets (*e.g.* Bragg) helps to minimise their influence on the refinement. Nonetheless, we proceeded to check whether or not the existence of a bimodal distribution was affected by the value of Q_{max} used to generate the $G(r)$ function. Changing Q_{max} varies strongly the location and periodicity of Fourier ripples but ought not to greatly affect the positions and intensities of any real features of the data (though one must keep in mind that reducing Q_{max} also reduces the real-space resolution Δr). To this end we calculated $G(r)$ data for 11 equally-spaced values $30 \leq Q_{max} \leq 50$ Å^{-1} (Fig. 4b) and used each of these modified data sets to drive an independent RMC refinement. On convergence, refinement was continued for sufficiently many RMC steps to obtain a minimum of seven independent configurations for each run (independent configurations being separated by 140 000 $\simeq$ 59 904 ln 10 accepted moves [34]).

For each of the 11 sets of RMC configurations produced in these refinements, the corresponding Cu2−O4 bond-length distributions were calculated and fitted as described above. It was found that two Gaussian functions were *always* required for these fits and that the corresponding Gaussian midpoints did not vary particularly strongly with Q_{max} (Fig. 3b). The values of the short and long Cu2−O4 bond lengths we obtain as averages over the various configurations are compared with the EXAFS results of Ref. [12] in Table 3. To give an idea of the level of confidence in these values, we have shown examples of the distributions corresponding to both the most and the least convincing bimodal fits (Fig. 3a). There is consistency also in the Gaussian widths and peak areas: in both cases the values obtained across all 11 data sets vary by less than 10%. Taking an error-weighted average across all 11 sets of configurations, we obtain a fraction of short Cu2−O4 bonds of $12.3 \pm 2.8\%$. For completeness, we note that it is not at all unexpected that the bond lengths

This article is protected by German copyright law. You may copy and distribute this article for your personal use only. Other use is only allowed with written permission by the copyright holder.

Table 3. Atom positional parameters and Cu2−O4 bond lengths determined using various experimental techniques and refinement strategies.

	Rietveld		PDFGui		RMC	EXAFS
	this work	Ref. [15]	this work	Ref. [21]	this work	Ref. [12]
z_{Ba}	0.18377(12)	0.18369(12)	0.1836(9)	0.1840(2)	0.18398(9)	–
z_{Cu2}	0.35535(9)	0.35464(8)	0.357(5)	0.3548(2)	0.35580(7)	–
z_{O2}	0.37837(13)	0.37808(7)	0.3778(29)	0.3780(3)	0.37701(11)	–
z_{O3}	0.37727(15)	0.37808(7)	0.378(2)	0.3782(3)	0.37805(8)	–
z_{O4}	0.15879(11)	0.15919(10)	0.1600(9)	0.1599(2)	0.15951(9)	–
$\langle d(\text{Cu2}-\text{O4})\rangle$ (Å)	2.2879(17)	2.2860(15)	2.268(14)	2.280(3)	2.2849(13)	–
$d(\text{Cu2}-\text{O4})_{\text{short}}$ (Å)	–	–	2.20(10)	2.19(3)	2.197(10)	2.220(5)
$d(\text{Cu2}-\text{O4})_{\text{long}}$ (Å)	–	–	2.29(10)	2.37(3)	2.306(3)	2.337(5)

extracted for the lowest and highest Q_{max} values are the least reliable: in the former case, the real-space resolution Δr is heavily reduced, and in the latter case the incorporation of high-Q noise begins to affect noticeably the smoothness of the $G(r)$ function.

3.3 PDFgui refinements

In order to ensure consistency with previous PDF studies, we performed a final set of PDF refinements using the PDFgui software package [36]. Sometimes termed a 'real-space Rietveld' approach, PDFgui uses the experimental $G(r)$ function to refine atomic coordinates and displacement parameters within a single unit cell. Our aim here was to reproduce the results of Ref. [21]: namely, that a split site could be refined for the Cu2 atom but not for the apical O4 atom, and that the split Cu2 atom sites corresponded to a difference Δd(Cu2−O4) between 'short' and 'long' Cu2−O4 bond lengths of 0.18(6) Å.

Our PDFgui refinements yielded the fit shown in Fig. 5, where we have used a Q_{max} value of 25 Å^{-1} in order to replicate the conditions of Ref. [21]. It was noted in this earlier study that the range of r values included in the fitting process had a significant effect on the value of Δd(Cu2−O4) obtained; this r-dependency in PDFgui refinements is symptomatic of the existence of short-range correlations that are not well described by the long-range structural periodicity (see *e.g.* Ref. [37]). Consequently, we determined values of Δd(Cu2−O4) for the two values employed in Ref. [21] ($r_{max} = 5$ and 15 Å) and also for a range of $G(r)$ functions generated using increasingly large Q_{max} values; our results are given in Tables 3 and 4.

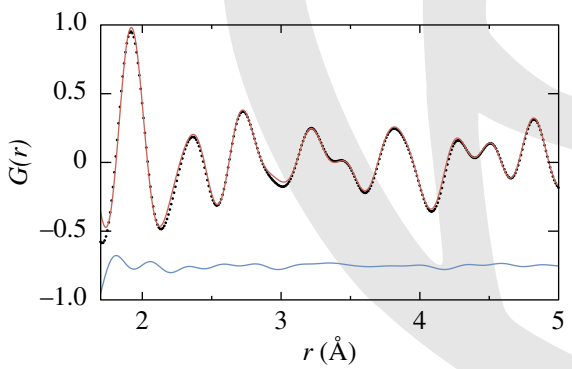

Fig. 5. A typical fit to $G(r)$ data obtained using PDFgui, in this instance for the experimental $G(r)$ function obtained using $Q_{max} = 25$ Å^{-1}.

Table 4. Differences Δd(Cu2−O4) between short and long Cu2−O4 bond lengths determined using r-dependent PDFgui refinement of the experimental $G(r)$ functions generated for various Q_{max} values. R_{ws} and R_{wu} as defined in Ref. [21].

Q_{max} (Å^{-1})	r_{max} (Å)	Δd(Cu2−O4) (Å)	R_{ws}	R_{wu}
25	5	0.08(7)	0.0908	0.0935
	15	0.03(5)	0.0883	0.0901
30	5	0.089(26)	0.1224	0.1406
	15	0.03(6)	0.0941	0.0951
40	5	0.099(28)	0.1207	0.1267
	15	0.065(26)	0.1261	0.1276
50	5	0.093(22)	0.1863	0.1888
	15	0.008(4)	0.2146	0.2157

While we found that it was possible to refine split sites for the Cu2 atom, the difference between 'long' and 'short' Cu2−O4 bonds was slightly smaller than that reported in Ref. [21]. Like the earlier study, we also found that split-site refinements gave improved fits when only the lowest-r region of the PDF was used, suggesting that the effects of site splitting only impact noticeably on the PDF over short distances. We note that, for some of the various combinations of Q_{max} and r_{max}, it was actually possible to refine a split O4 site; however the corresponding distance between sites was never larger than 0.05 Å.

4. Discussion

Perhaps the key result of our RMC study is to demonstrate that a single atomistic configuration can account at once for a number of the seemingly disparate experimental results reported previously for $YBa_2Cu_3O_{7-\delta}$:

1. The finding from both single crystal and powder diffraction studies that the scattering distributions at the Cu2 and O4 sites of the average structure are unimodal [14–19].
2. That two Cu2−O4 bond lengths are required to obtain satisfactory fits to Cu K-edge EXAFS spectra [9–13].

This article is protected by German copyright law. You may copy and distribute this article for your personal use only. Other use is only allowed with written permission by the copyright holder.

3. For PDFgui refinements over small regions in real space ($r_{max} \simeq 5$ Å), neutron PDF data are best fitted in terms of a structural model with two Cu2 sites (and hence two Cu2−O4 distances); however as r_{max} is increased the refined splitting between Cu2 sites vanishes [21].
4. The magnitude of the splitting is much larger than the U_{33} parameter of the Cu2 atom.

Consistency between a bimodal Cu2−O4 bond length distribution on the one hand, and single Cu2/O4 sites in the average structure on the other hand, demands that the Cu2 and O4 displacements are correlated during short- and long-bond formation. Specifically, shortening of the Cu2−O4 bond must involve cooperative displacement of the Cu2 atom in the $-z$ direction (with reference to the coordinates and axes of Fig. 1a) and of the O4 atom in the $+z$ direction; lengthening of the same bond must involve correlated displacement in the opposite direction. A model that involves both a split Cu2 site and a split O4 site is not supported by Rietveld refinement as the displacements from the equilibrium positions will be indistinguishable from thermal motion [38]. Such a model would also produce a trimodal Cu2−O4 distribution [39] if correlations were not taken into account, which is clearly inconsistent with the PDF results.

For the low-r_{max} PDFgui refinements, a Cu2 split site model allows the bimodal Cu2−O4 bond distribution to be successfully fitted, but does so with a model that is more difficult to resolve with the average structure − if the distortion is taken up by the Cu2 site alone then the U_{33} atomic displacement parameter for Cu2 would be larger than is observed. The RMC model confirms the bimodal Cu2−O4 bond distribution found previously, but by sharing the distortions between the two sites in a correlated manner it is explicitly consistent with average structure models.

There will be a temptation to associate with the two Cu2−O4 bond types a different valence state for the Cu2 atom; certainly the difference in bond length (0.11 Å) is not inconsistent with a change in Cu oxidation state. We note, however, that the neutron PDF measurements we have performed here involve no scattering contribution from the electronic structure of the material and hence we do not comment further on this aspect.

We might expect our RMC configurations to be somewhat sensitive to correlations in the spatial arrangement of the different types of Cu2−O4 bonds, should any such distortion exist. We have been made aware of an earlier, unpublished, RMC study in which short-bond/short-bond correlations are discussed [40], and we conclude here with a similar calculation for our own RMC configurations. In order to quantify the extent to which short Cu2−O4 bonds are found to cluster, we define a correlation function

$$\chi(r) = \frac{a_{\rm eff}}{Nr} \sum_i \sum_j u_i u_j(r)\,, \qquad (4)$$

where

$$u_i = \begin{cases} +1 & d(\text{Cu2}-\text{O4})_i > d_c \\ -1 & d(\text{Cu2}-\text{O4})_i > d_c \end{cases}, \qquad (5)$$

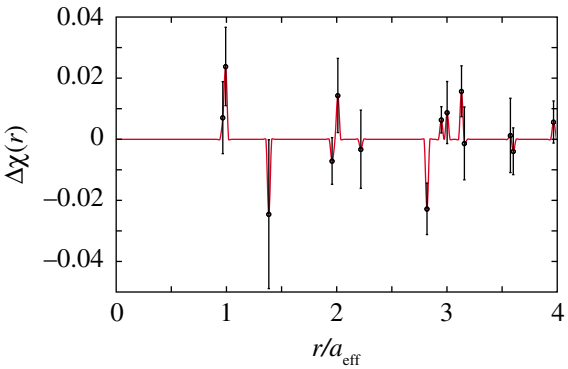

Fig. 6. The short-bond/short-bond correlation function $\Delta\chi(r)$ calculated for eight RMC configurations and then averaged. For ease of interpretation, the horizontal axis corresponds to interatomic distances scaled relative to the average in-plane lattice parameter. The positive peak at $r/a_{\rm eff} = 1$ indicates that short apical Cu2−O4 bonds may prefer to form neighbouring pairs.

$a_{\rm eff} = \sqrt{ab}$, the distance d_c is the critical Cu2−O4 bond length below which a bond is considered to be 'short', N is the number of Cu2 centres in a configuration, and the sums in Eq. (4) are taken over all Cu2 centres i,j within the same $[CuO_2]$ layer and separated by the distance r. Because the number of short and long bonds differ, $\chi(r)$ will generally be non-zero even for random distributions of short bonds; consequently we calculate also a statistical correlation function $\chi_{\rm rand}(r)$ which is generated using the same set of u_i values as $\chi(r)$, but with these distributed randomly throughout the configuration. Then the difference function

$$\Delta\chi(r) = \chi(r) - \chi_{\rm rand}(r) \qquad (6)$$

measures the extent to which short Cu2−O4 bonds are more ($\Delta\chi(r) > 0$) or less ($\Delta\chi(r) < 0$) likely to cluster at a distance r than in a random distribution.

The $\Delta\chi(r)$ function was calculated for 8 configurations and then averaged to produce the correlation function shown in Fig. 6. The degree of variation in $\Delta\chi(r)$ we observe across our configurations is of the same order of magnitude as the function itself. Consequently, we do not attribute a great deal of significance to any peak−indeed few peaks lie more than two standard deviations away from zero (see Figs. S2–4 in the SI). Any tendency for short Cu2−O4 bonds to cluster into pairs (hinted at by the positive peak at $r/a_{\rm eff} = 1$) could be considered consistent with a bipolaron model, if accompanied by charge localisation [6].

In conclusion, RMC refinements of neutron PDF data collected for a $YBa_2Cu_3O_{6.93}$ sample yield atomistic configurations that are simultaneously consistent with all features of the short-range and long-range structural features captured by total scattering experiments and with the results of independent X-ray absorption spectroscopy experiments. We find that the apical Cu2−O4 bonds are of two types: a short bond of 2.197(10) Å and a long bond of 2.306(3) Å. We find no strong evidence for clustering of the short Cu2−O4 bonds within $[CuO_2]$ layers.

Acknowledgements. The authors are pleased to acknowledge valuable discussions with R. L. McGreevy. This research was supported finan-

This article is protected by German copyright law. You may copy and distribute this article for your personal use only. Other use is only allowed with written permission by the copyright holder.

cially by the EPSRC (grant EP/G004528/2) and the ERC (project 279705), and by the STFC in the form of access to the GEM instrument at ISIS.

References

[1] D. M. Newns, C. C. Tsuei, *Nature Phys.* **2007**, *3*, 184.
[2] D. Reznik, L. Pintschovius, M. Ito, S. Iikubo, M. Sato, H. Goka, M. Fujita, K. Yamada, G. D. Gu, J. M. Tranquada, *Nature* **2006**, *440*, 1170.
[3] J. Orenstein, A. J. Millis, *Science* **2000**, *288*, 468.
[4] C. Gadermaier, A. S. Alexandrov, V. V. Kabanov, P. Kusar, T. Mertelj, X. Yao, C. Manzoni, D. Brida, G. Cerullo, D. Mihailovic, *Phys. Rev. Lett.* **2010**, *105*, 257001.
[5] J. M. Tranquada, B. J. Sternlieb, J. D. Axe, Y. Nakamura, S. Uchida, *Nature* **1995**, *375*, 561.
[6] A. S. Alexandrov, *Phys. Scr.* **2011**, *83*, 038301.
[7] C. Q. Jin, Q. Q. Liu, H. Yang, L. X. Yang, R. C. Yu, F. Y. Li, *Physica C* **2007**, *460*, 178.
[8] S. D. Conradson, I. D. Raistrick, *Science* **1989**, *243*, 1340.
[9] J. Mustre de Leon, S. D. Conradson, I. Batištić, A. R. Bishop, *Phys. Rev. Lett.* **1990**, *65*, 1675.
[10] J. Mustre de Leon, S. D. Conradson, I. Batištić, A. R. Bishop, I. D. Raistrick, M. C. Aronson, F. H. Garzon, *Phys. Rev. B* **1992**, *45*, 2447.
[11] E. A. Stern, M. Qian, Y. Yacoby, S. M. Heald, H. Maeda, *Physica C: Superconduct.* **1993**, *209*, 331.
[12] C. H. Booth, F. Bridges, J. B. Boyce, T. Claeson, B. M. Lairson, R. Liang, D. A. Bonn, *Phys. Rev. B* **1996**, *54*, 9542.
[13] T. A. Tyson, J. F. Federici, D. Chew, A. R. Bishop, L. Furenlid, W. Savin, W. Wilber, *Physica C* **1997**, *292*, 163.
[14] J. D. Sullivan, P. Bordet, M. Marezio, K. Takenaka, S. Uchida, *Phys. Rev. B* **1993**, *48*, 10638.
[15] P. Schweiss, W. Reichardt, M. Braden, G. Collin, G. Heger, H. Claus, A. Erb, *Phys. Rev. B* **1994**, *49*, 1387.
[16] M. François, A. Junod, K. Yvon, A. W. Hewat, J. J. Capponi, P. Strobel, M. Marezio, P. Fischer, *Solid State Commun.* **1988**, *66*, 1117.
[17] A. Williams, G. H. Kwei, R. B. Von Dreele, A. C. Larsen, I. D. Raistrick, D. L. Bish, *Phys. Rev. B* **1988**, *37*, 7960.
[18] G. H. Kwei, A. C. Larson, W. L. Hults, J. L. Smith, *Physica C* **1990**, *169*, 217.
[19] G. H. Kwei, A. C. Larson, W. L. Hults, J. L. Smith, *Physica C* **1991**, *175*, 615.
[20] D. Louca, G. H. Kwei, B. Dabrowski, Z. Bukowski, *Phys. Rev. B* **1999**, *60*, 7558.
[21] M. Gutmann, S. J. L. Billinge, E. L. Brosha, G. H. Kwei, *Phys. Rev. B* **2000**, *61*, 11762.
[22] A. I. Liechtenstein, I. I. Mazin, O. K. Anderson, O. Jepsen, *Phil. Mag. B* **1994**, *70*, 643.
[23] M. Arai, K. Yamada, S. Hosoya, A. C. Hannon, Y. Hidaka, A. D. Taylor, Y. Endoh, *J. Superconduct.* **1994**, *7*, 415.
[24] D. H. A. Blank, H. Kruidhof, J. Flokstra, *J. Phys. D: Appl. Phys.* **1988**, *21*, 226.
[25] R. P. Sharma, F. J. Rotella, J. D. Jorgensen, L. E. Rehn, *Physica C: Superconduct.* **1991**, *174*, 409.
[26] W. G. Williams, R. M. Ibberson, P. Day, J. E. Enderby, *Physica B: Condens. Matt.* **1998**, *241*, 234.
[27] P. Day, J. Enderby, W. Williams, L. Chapon, A. Hannon, P. Radaelli, A. Soper, *Neutron News* **2004**, *15*, 19.
[28] A. C. Hannon, *Nucl. Instrum. Methods Phys. Res. A* **2005**, *551*, 88.
[29] M. T. Dove, M. G. Tucker, D. A. Keen, *Eur. J. Miner.* **2002**, *14*, 331.
[30] D. A. Keen, *J. Appl. Crystallogr.* **2001**, *34*, 172.
[31] A. C. Larson, R. B. Von Dreele, *Los Alamos National Laboratory Report LAUR 86–748* **1994**.
[32] J. J. Capponi, C. Chaillout, A. W. Hewat, P. Lejay, M. Marezio, N. Nguyen, B. Raveau, J. L. Soubeyroux, J. L. Tholence, R. Tournier, *Europhys. Lett.* **1987**, *3*, 1301.
[33] M. G. Tucker, D. A. Keen, M. T. Dove, A. L. Goodwin, Q. Hui, *J. Phys.: Condens. Matt.* **2007**, *19*, 335218.
[34] A. L. Goodwin, M. G. Tucker, E. R. Cope, M. T. Dove, D. A. Keen, *Phys. Rev. B* **2005**, *72*, 214304.
[35] T. Egami, S. J. L. Billinge, *Underneath the Bragg peaks: structural analysis of complex materials*, Pergamon, London **2003**.
[36] C. L. Farrow, P. Juhas, J. W. Liu, D. Bryndin, E. S. Božin, J. Bloch, T. Proffen, S. J. L. Billinge, *J. Phys.: Condens. Matt.* **2007**, *19*, 335219.
[37] E. S. Bozin, M. Schmidt, A. J. DeConinck, G. Paglia, J. F. Mitchell, T. Chatterji, P. G. Radaelli, T. Proffen, S. J. L. Billinge, *Phys. Rev. Lett.* **2007**, *98*, 137203.
[38] We note that our Rietveld refinement gives the root-mean-squared displacement of the Cu2 and O4 atoms in the z direction to be 0.066 and 0.070 Å, respectively; consequently displacements of $\frac{1}{2}\Delta d(\mathrm{Cu2-O4}) \simeq 0.055$ Å away from each site would be indistinguishable from thermal motion.
[39] Near Cu2, near O4; near Cu2, far O4 / far Cu2, near O4; far Cu2, far O4.
[40] See the comment by R. L. McGreevy in A. S. Alexandrov, *Phil. Trans. R. Soc. Lond. A* **1998**, *356*, 197.

This article is protected by German copyright law. You may copy and distribute this article for your personal use only. Other use is only allowed with written permission by the copyright holder.

Reverse Monte Carlo study of apical Cu–O bond distortions in $YBa_2Cu_3O_{6.93}$: Supplementary Information

Callum A. Young,[1] Edward Dixon,[1] Matthew G. Tucker,[2] David A. Keen,[2] Michael A. Hayward,[1] and Andrew L. Goodwin[1,*]

[1] *Department of Chemistry, University of Oxford, Inorganic Chemistry Laboratory, South Parks Road, Oxford OX1 3QR, U.K.*

[2] *ISIS Facility, Rutherford Appleton Laboratory, Harwell Oxford, Didcot OX11 0QX, U.K.*

(Dated: January 27, 2012)

* andrew.goodwin@chem.ox.ac.uk

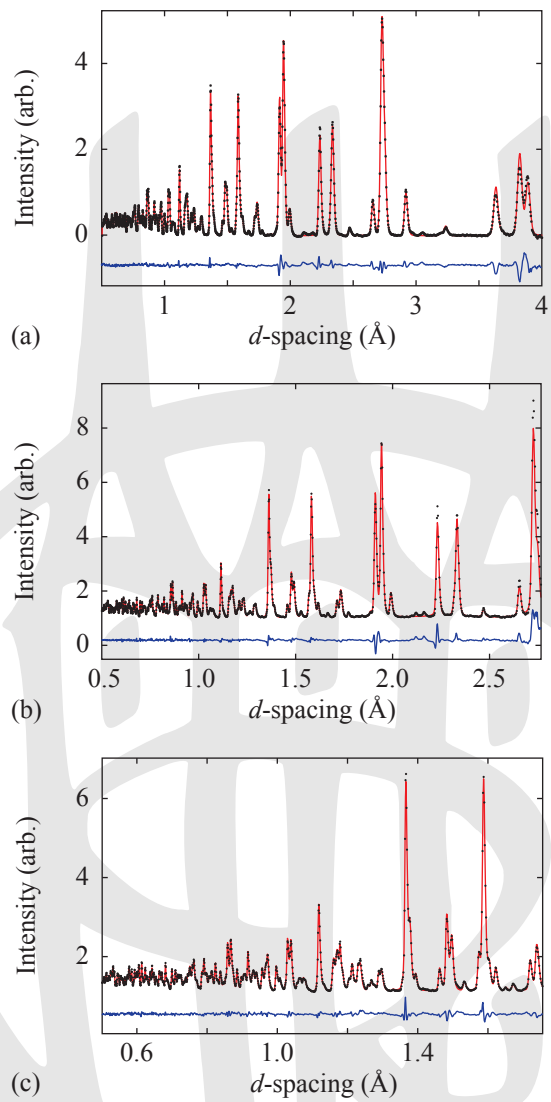

FIG. 1: Rietveld refinements for the separate GEM detector banks. (a) Bank 4, $2\theta = 54.46°$; (b) Bank 5, 63.62°; (c) Bank 6, 91.37°. The final fit gave residuals $wR_p = 0.0207$ and $R_p = 0.0218$.

This article is protected by German copyright law. You may copy and distribute this article for your personal use only. Other use is only allowed with written permission by the copyright holder.

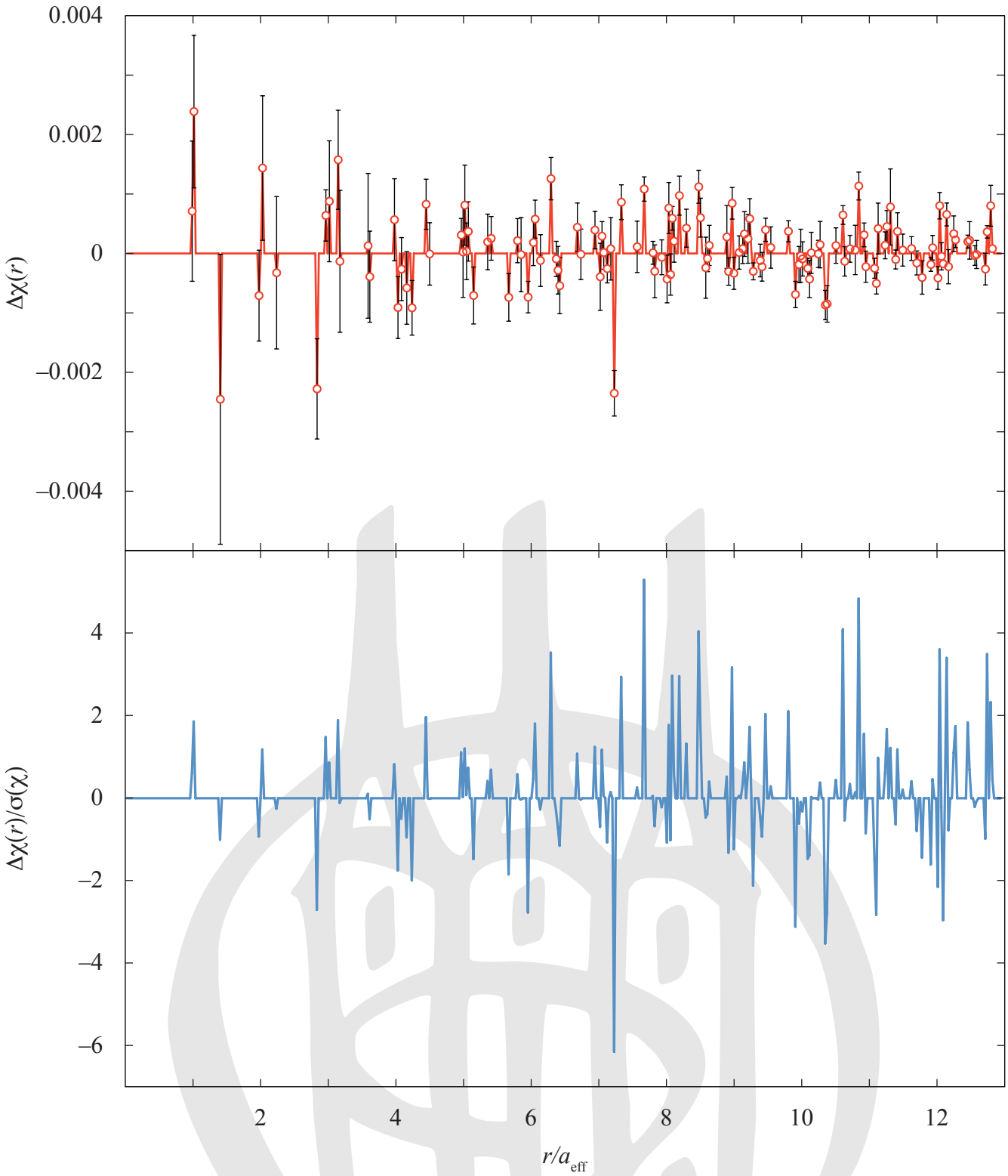

FIG. 2: The correlation function $\Delta\chi(r)$ plotted out to $r/a_{\rm eff} = 13$ (above); a plot of the correlation function divided by its standard error, to give an indication of the significance of each peak (below).

This article is protected by German copyright law. You may copy and distribute this article for your personal use only. Other use is only allowed with written permission by the copyright holder.

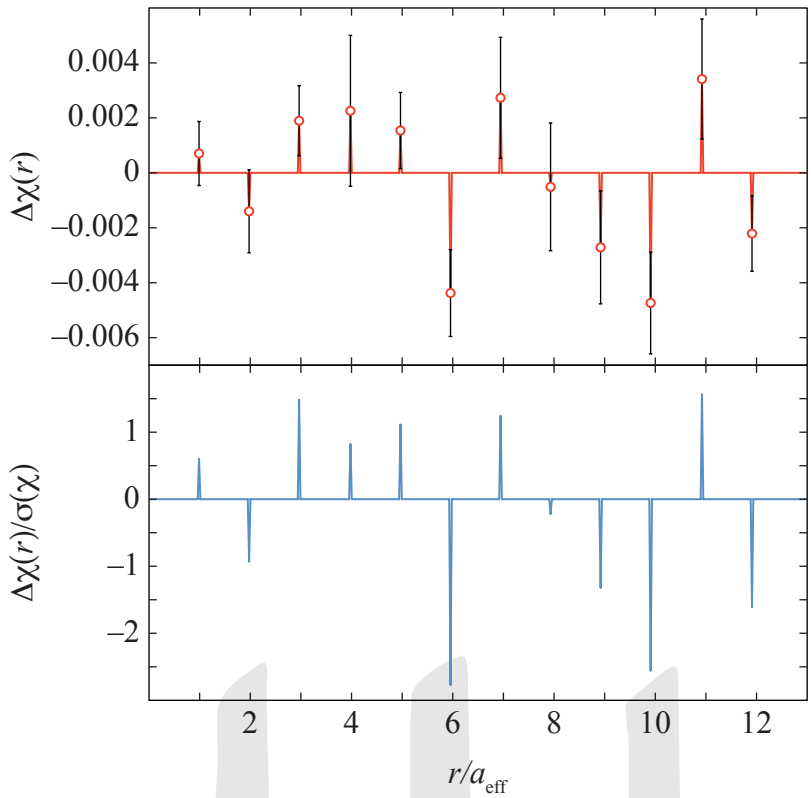

FIG. 3: The correlation function along the x-direction alone (above), and divided by its error (below).

This article is protected by German copyright law. You may copy and distribute this article for your personal use only. Other use is only allowed with written permission by the copyright holder.

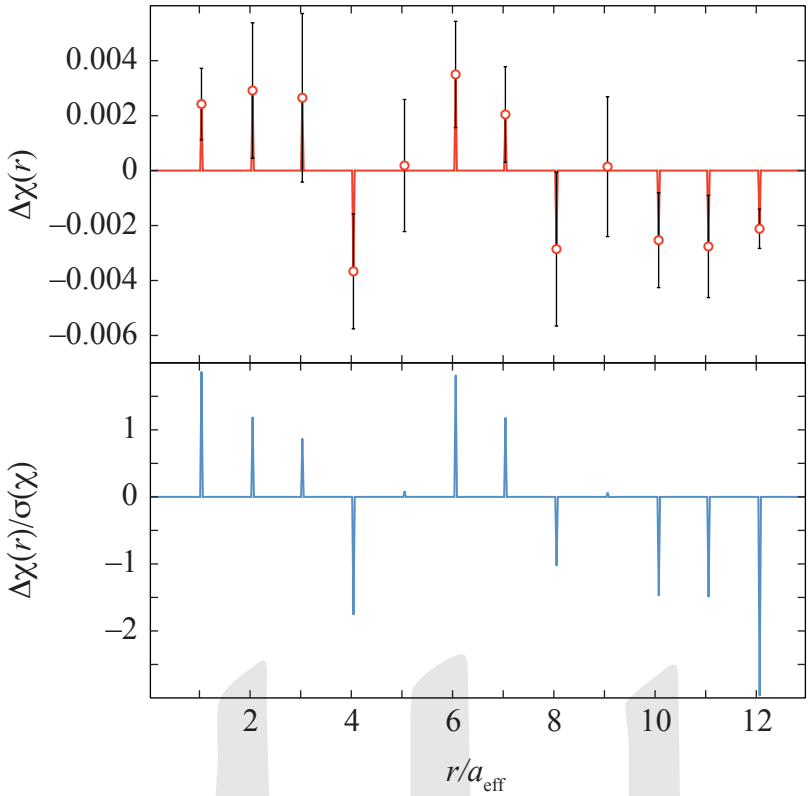

FIG. 4: The correlation function along the y-direction alone (above), and divided by its error (below).

This article is protected by German copyright law. You may copy and distribute this article for your personal use only. Other use is only allowed with written permission by the copyright holder.